Chapter 7
Computational Results

In this chapter, we perform six sets of experiments to evaluate the effectiveness of the APCDM and its submodels and their respective sensitivities to various parameters.

First, we examine the performance of our stochastic approach towards generating aircraft trajectory realizations and conducting the overall conflict analysis. In addition to testing several probabilistic trajectory displacement distributions, we establish a set of baseline threshold probabilities used to define whether a significant conflict risk exists between any pair of flight plans.

The second set of experiments verify the effectiveness of the C_3 and C_4 conflict constraint formulations, as defined in Chapter 4. We show that the C_4 formulation is more effective, in terms of computational effort, than the C_3 formulation.

Following this analysis, three other sets of experiments are dedicated to testing the APCDM solution sensitivity to the CDM-related parameters that were defined in Chapter 5, specifically, $D_{\max}$, $E^e_{\max}$, and μ_0. Finally, we perform a sensitivity analysis for the three conflict threshold probabilities by varying them from their respective baseline values. We report the respective impacts on the optimal solution generated by the APCDM in terms of the objective function value, flight cancellation rate, airline-optimized surrogate utilization rate, as well as the levels of ω-mean collaboration efficiency and collaboration equity achieved.

All reported computations have been made on a Dell Inspiron 7500 laptop computer equipped with a 650 MHz Pentium III processor and 192 Mb Random Access Memory, and utilizing the Microsoft Windows 2000 operating system. The various submodels were programmed using Microsoft Visual C++ Version 6 and the APCDM mixed-integer programs were solved using CPLEX 7.0.

The various data sets were constructed beginning with the Enhanced Traffic Management System (ETMS) flight data information. For each flight taken from this database, several alternate trajectories were generated between the respective origin-destination pair. Then, for each of these alternative trajectories plus the original flight plan, multiple surrogates were generated, with the respective take-off times modified by chosen lengths of time. For example, to generate a suitable data set for APCDM experimentation, we might generate two alternative trajectories for each flight to be taken, and for each of these, we might adopt three alternative scheduled take-off times, thus yielding a total of six surrogates for each flight (a "cancellation surrogate" is additionally generated as well).

7.1. Analysis of the PAEM Model

7.1.1. Preliminary Test Data

The APCDM and the several submodels were tested using sets of flight plans scheduled to traverse the Miami-Jacksonville ARTCCs. Two data sets, specified in Table 7-1, were used for the initial analysis of the PAEM model.

	Test Set 1		**Test Set 2**	
Number of Flights	30		80	
Surrogates per Flight	6		6	
Center(s)	ZMA/ZJX		ZMA/ZJX	
Number of Airlines	5		5	
Airlines: Flights per Airline	AAL: ABX/ACA/AMT: CAA: COA: DAL:	10 5 7 3 5	AAL: ABX/ACA/AMT: CAA: COA: DAL:	18 5 7 25 25
Time Horizon	1200 min		1200 min	
Number of Deterministic Conflicts Identified	Level 1: Level 2: Fatal:	69 15 0	Level 1: Level 2: Fatal:	559 235 5

Table 7-1: Preliminary Test Data Sets

7.1.2. Probabilistic Trajectory Displacement Realizations

As discussed in Chapter 3, we experimented with two types of probabilistic trajectory displacements regions: rectangular and cylindrical. The first set of trajectory displacement realizations was developed in Section 3.2.1. for a rectangular bounded region and is shown again in Table 7-2 for convenience.

ξ_{Ak}^{q} (nm)	p_{Ak}	ξ_{Ak}^{q} (nm)	p_{Ak}	ξ_{Ak}^{q} (nm)	p_{Ak}
2.933, -0.333, -0.044	0.008889	1.511, 0.333, -0.044	0.026666	-1.511, 0, -0.044	0.026666
2.933, -0.333, 0	0.008889	1.511, 0.333, 0	0.026666	-1.511, 0, 0	0.026666
2.933, -0.333, 0.044	0.008889	1.511, 0.333, 0.044	0.026666	-1.511, 0, 0.044	0.026666
2.933, 0, -0.044	0.008889	0, -0.333, -0.044	0.04	-1.511, 0.333, -0.044	0.026666
2.933, 0, 0	0.008889	0, -0.333, 0	0.04	-1.511, 0.333, 0	0.026666
2.933, 0, 0.044	0.008889	0, -0.333, 0.044	0.04	-1.511, 0.333, 0.044	0.026666
2.933, 0.333, -0.044	0.008889	0, 0, -0.044	0.04	-2.933, -0.333, -0.044	0.008889
2.933, 0.333, 0	0.008889	0, 0, 0	0.04	-2.933, -0.333, 0	0.008889
2.933, 0.333, 0.044	0.008889	0, 0, 0.044	0.04	-2.933, -0.333, 0.044	0.008889
1.511, -0.333, -0.044	0.026666	0, 0.333, -0.044	0.04	-2.933, 0, -0.044	0.008889
1.511, -0.333, 0	0.026666	0, 0.333, 0	0.04	-2.933, 0, 0	0.008889
1.511, -0.333, 0.044	0.026666	0, 0.333, 0.044	0.04	-2.933, 0, 0.044	0.008889
1.511, 0, -0.044	0.026666	-1.511, -0.333, -0.044	0.026666	-2.933, 0.333, -0.044	0.008889
1.511, 0, 0	0.026666	-1.511, -0.333, 0	0.026666	-2.933, 0.333, 0	0.008889
1.511, 0, 0.044	0.026666	-1.511, -0.333, 0.044	0.026666	-2.933, 0.333, 0.044	0.008889

Table 7-2: Trajectory Displacement Set 1 (Rectangular Region, 45 Realizations)

The second trajectory displacement set shown in Table 7-3 uses the same rectangular bounded displacement region as the first set, but is instead discretized into 27 subregions. The third set eliminates consideration of altitude displacements from the first set, and hence encompasses only 15 planar realizations.

ξ_{Ak}^{q} (nm)	p_{Ak}	ξ_{Ak}^{q} (nm)	p_{Ak}	ξ_{Ak}^{q} (nm)	p_{Ak}
-2.767, -0.333, -0.044	0.0185	-2.767, -0.333, 0	0.0185	-2.767, -0.333, 0.044	0.0185
-2.767, 0, -0.044	0.0185	-2.767, 0 , 0	0.0185	-2.767, 0, 0.044	0.0185
-2.767, 0.333, -0.044	0.0185	-2.767, 0.333, 0	0.0185	-2.767, 0.333, 0.044	0.0185
0, -0.333, -0.044	0.0463	0, -0.333, 0	0.0463	0, -0.333, 0.044	0.0463
0, 0, -0.044	0.0463	0, 0 , 0	0.0463	0, 0, 0.044	0.0463
0, 0.333, -0.044	0.0463	0, 0.333, 0	0.0463	0, 0.333, 0.044	0.0463
2.767, -0.333, -0.044	0.0185	2.767, -0.333, 0	0.0185	2.767, -0.333, 0.044	0.0185
2.767, 0, -0.044	0.0185	2.767, 0 , 0	0.0185	2.767, 0, 0.044	0.0185
2.767, 0.333, -0.044	0.0185	2.767, 0.333, 0	0.0185	2.767, 0.333, 0.044	0.0185

Table 7-3: Trajectory Displacement Set 2 (Rectangular Region, 27 Realizations)

ξ_{Ak}^{q} (nm)	p_{Ak}	ξ_{Ak}^{q} (nm)	p_{Ak}	ξ_{Ak}^{q} (nm)	p_{Ak}
-2.933, -0.333, 0	0.0267	-2.933, 0, 0	0.0267	-2.933, 0.333, 0	0.0267
-1.511, -0.333, 0	0.08	-1.511, 0, 0	0.08	-1.511, 0.333, 0	0.08
0, -0.333, 0	0.12	0, 0, 0	0.12	0, 0.333, 0	0.12
1.511, -0.333, 0	0.08	1.511, 0, 0	0.08	1.511, 0.333, 0	0.08
2.933, -0.333, 0	0.0267	2.933, 0, 0	0.0267	2.933, 0.333, 0	0.0267

Table 7-4: Trajectory Displacement Set 3 (Rectangular Planar, 15 Realizations)

The fourth trajectory displacement set was developed in Section 3.2.2. for a cylindrical bounded region. In contrast with Table 3-2, Table 7-5 shows the displacements in the format they are input to the PAEM. The trajectory displacement sets for cylindrical bounded regions were derived using two different unitized wind vectors. The first, $w = [0.3084, 0.4856, 0.8180]$, corresponds to an approximate south-southwesterly wind and the second, $w = [0.0786, 0.4489, 0.8896]$, corresponds to an approximately northerly wind, both measured at Palm Beach International (FL) Airport.

Table 7-6 records the Trajectory Displacement Set 5, which is defined as the planar version of Trajectory Displacement Set 4.

(r_k, Δ_k, h_k)	p_{Ak}	(r_k, Δ_k, h_k)	p_{Ak}	(r_k, Δ_k, h_k)	p_{Ak}
0.476, -0.0582, -0.044	0.0486	0.476, -0.0582, 0	0.0486	0.476, -0.0582, 0.044	0.0486
0.476, 0, -0.044	0.0486	0.476, 0, 0	0.0486	0.476, 0, 0.044	0.0486
0.476, 0.0582, -0.044	0.0486	0.476, 0.0582, 0	0.0486	0.476, 0.0582, 0.044	0.0486
1.467, -0.0582, -0.044	0.0347	1.467, -0.0582, 0	0.0347	1.467, -0.0582, 0.044	0.0347
1.467, 0, -0.044	0.0347	1.467, 0, 0	0.0347	1.467, 0, 0.044	0.0347
1.467, 0.0582, -0.044	0.0347	1.467, 0.0582, 0	0.0347	1.467, 0.0582, 0.044	0.0347
2.444, -0.0582, -0.044	0.0208	2.444, -0.0582, 0	0.0208	2.444, -0.0582, 0.044	0.0208
2.444, 0, -0.044	0.0208	2.444, 0, 0	0.0208	2.444, 0, 0.044	0.0208
2.444, 0.0582, -0.044	0.0208	2.444, 0.0582, 0	0.0208	2.444, 0.0582, 0.044	0.0208
3.333, -0.0582, -0.044	0.0069	3.333, -0.0582, 0	0.0069	3.333, -0.0582, 0.044	0.0069
3.333, 0, -0.044	0.0069	3.333, 0, 0	0.0069	3.333, 0, 0.044	0.0069
3.333, 0.0582, -0.044	0.0069	3.333, 0.0582, 0	0.0069	3.333, 0.0582, 0.044	0.0069

Table 7-5: Trajectory Displacement Set 4 (Cylindrical Region, 36 Realizations)

(r_k, Δ_k, h_k)	p_{Ak}	(r_k, Δ_k, h_k)	p_{Ak}	(r_k, Δ_k, h_k)	p_{Ak}
0.476, -0.0582, 0	0.1458	0.476, 0, 0	0.1458	0.476, 0.0582, 0	0.1458
1.467, -0.0582, 0	0.1041	1.467, 0, 0	0.1041	1.467, 0.0582, 0	0.1041
2.444, -0.0582, 0	0.0624	2.444, 0, 0	0.0624	2.444, 0.0582, 0	0.0624
3.333, -0.0582, 0	0.0207	2.444, 0, 0	0.0207	2.444, 0.0582, 0	0.0207

Table 7-6: Trajectory Displacement Set 5 (Circular Planar, 12 Realizations)

Finally, Tables 7-7, 7-8, and 7-9 show three additional trajectory displacement sets that were used in our initial experiment, for a total of 11 randomized error scenarios, for each of the two test data sets given in Table 7-1.

ξ_{Ak}^{q} (nm)	p_{Ak}	ξ_{Ak}^{q} (nm)	p_{Ak}	ξ_{Ak}^{q} (nm)	p_{Ak}
-3.238, -0.333, 0	0.0136	-3.238, 0, 0	0.0136	-3.238, 0.333, 0	0.0136
-2.222, -0.333, 0	0.0408	-2.222, 0, 0	0.0408	-2.222, 0.333, 0	0.0408
-1.104, -0.333, 0	0.0680	-1.104, 0, 0	0.0680	-1.104, 0.333, 0	0.0680
0, -0.333, 0	0.0884	0, 0, 0	0.0884	0, 0.333, 0	0.0884
1.104, -0.333, 0	0.0680	1.104, 0, 0	0.0680	1.104, 0.333, 0	0.0680
2.222, -0.333, 0	0.0408	2.222, 0, 0	0.0408	2.222, 0.333, 0	0.0408
3.238, -0.333, 0	0.0136	3.238, 0, 0	0.0136	3.238, 0.333, 0	0.0136

Table 7-7: Trajectory Displacement Set 6 (Rectangular Planar, 21 Realizations)

ξ_{Ak}^{q} (nm)	p_{Ak}	ξ_{Ak}^{q} (nm)	p_{Ak}	ξ_{Ak}^{q} (nm)	p_{Ak}
-3.515, -0.333, 0	0.0055	-3.515, 0, 0	0.0055	-3.515, 0.333, 0	0.0055
-2.867, -0.333, 0	0.0165	-2.867, 0, 0	0.0165	-2.867, 0.333, 0	0.0165
-2.158, -0.333, 0	0.0275	-2.158, 0, 0	0.0275	-2.158, 0.333, 0	0.0275
-1.437, -0.333, 0	0.0386	-1.437, 0, 0	0.0386	-1.437, 0.333, 0	0.0386
-0.714, -0.333, 0	0.0496	-0.714, 0, 0	0.0496	-0.714, 0.333, 0	0.0496
0, -0.333, 0	0.0579	0, 0, 0	0.0579	0, 0.333, 0	0.0579
0.714, -0.333, 0	0.0496	0.714, 0, 0	0.0496	0.714, 0.333, 0	0.0496
-.437, -0.333, 0	0.0386	1.437, 0, 0	0.0386	1.437, 0.333, 0	0.0386
2.158, -0.333, 0	0.0275	2.158, 0, 0	0.0275	2.158, 0.333, 0	0.0275
2.867, -0.333, 0	0.0165	2.867, 0, 0	0.0165	2.867, 0.333, 0	0.0165
3.515, -0.333, 0	0.0055	3.515, 0, 0	0.0055	3.515, 0.333, 0	0.0055

Table 7-8: Trajectory Displacement Set 7 (Rectangular Planar, 33 Realizations)

(r_k, Δ_k, h_k)	p_{Ak}	(r_k, Δ_k, h_k)	p_{Ak}	(r_k, Δ_k, h_k)	p_{Ak}
0.385, -0.0582, 0	0.1200	0.385, 0, 0	0.1200	0.385, 0.0582, 0	0.1200
1.181, -0.0582, 0	0.0933	1.181, 0, 0	0.0933	1.181, 0.0582, 0	0.0933
1.973, -0.0582, 0	0.0667	1.973, 0, 0	0.0667	1.973, 0.0582, 0	0.0667
2.756, -0.0582, 0	0.0400	2.756, 0, 0	0.0400	2.756, 0.0582, 0	0.0400
3.467, -0.0582, 0	0.0133	3.467, 0, 0	0.0133	3.467, 0.0582, 0	0.0133

Table 7-9: Trajectory Displacement Set 8 (Circular Planar, 15 Realizations)

7.1.3. Evaluation of the PAEM Model Performance

We examined the main PAEM algorithm's processing time for a given problem as a function of the number of probabilistic trajectory realizations (using both rectangular and cylindrical displacement regions) generated for the analysis. Recall from Section 3.5 that for each piecewise linear trajectory segment of the focal aircraft A's flight plan, a conflict analysis is performed for each intruder aircraft B for all pairs of trajectory realizations $(k_1, k_2) \in \{1, ..., n_A\} \times \{1, ..., n_B\}$ (where n_A=n_B is the number of probabilistic realizations).

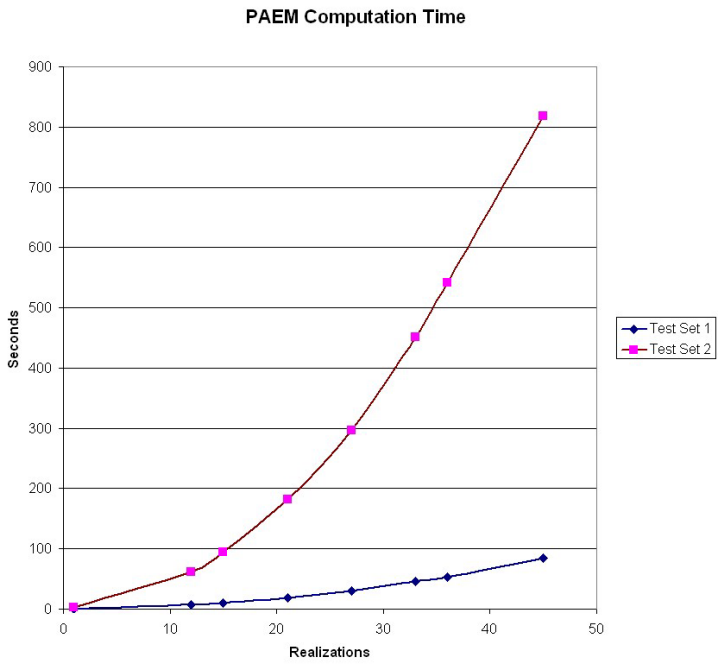

Figure 7-1: PAEM Processing Time Versus Number of Realizations

From Figure 7-1 we see that there is an increasing quadratic relationship between the number of realizations and the processing time. Clearly then, it is advantageous to limit the size of n_A, while maintaining representability of the probabilistic distribution of trajectories, when processing large data sets to retain a reasonable processing time. Note that other factors that influence the PAEM effort across different problem instances include the number of flights (and the number of surrogates proposed for each flight) to be processed, the nature of the respective flight plans (e.g., the number and duration of various flight segments), and the extent of potential pairwise conflicts, based on overlapping travel times and common assigned enroute flight levels.

Next, we examined the conflicts identified by the PAEM using each of the trajectory displacement sets. First, we noted that all the deterministic conflicts were identified in the probabilistic analyses, as expected, since the deterministic trajectories are included within the trajectory displacement sets as a probabilistic realization.

We compared the results using the three-dimensional displacement regions with the results using the counterpart two-dimensional displacements regions having the

same number of realizations in the horizontal plane (Displacement Set 1 versus 3 and Displacement Set 4 versus 5). Referring to the conflicts identified in the deterministic analysis, we observed that these conflicts occurred in the probabilistic analyses with an average conflict risk ranging from 0.30 to 0.32 in all four cases. Moreover, each pair of cases exhibited substantially similar (but not identical) conflict pairs.

Observe that for the three-dimensional displacement sets, the realizations are geometrically separated from each other by approximately 267 feet in the vertical dimension. Given the required vertical aircraft separations imposed by the FAA, we expect that these vertical displacements will not generate additional probabilistic conflicts unless one or both of the focal or intruder aircraft are ascending or descending. Our primary interest for the APCDM is in analyzing the alternative flight plans in the enroute airspace where aircraft are normally in level flight. Therefore, a reasonable tradeoff between accuracy in representation and PAEM processing effort is to eliminate consideration of vertical trajectory displacements.

Using the number of deterministic conflicts identified as a benchmark, we determined the number of conflicts identified (using Trajectory Displacement Sets 3 and 6) as the threshold probability parameter p_1 was varied (see the discussion of threshold probabilities in Section 3.4). Recall that the CTAS model of Erzberger, Paielli, Isaacson, and Eschow [16] nominally displays conflicts exceeding a (total) probability of 0.45. Table 7-10 displays the resulting data.

	Test Set 1		**Test Set 2**	
p_1	n_A **= 15**	n_A **= 21**	n_A **= 15**	n_A **= 21**
0.50	20	20	178	157
0.45	27	22	264	230
0.40	45	44	373	369
0.35	59	60	495	527
1/3	68	64	583	600
0.30	78	80	728	726
0.25	103	115	991	974

Table 7-10: Level 1 Conflicts Versus Threshold Probability

We chose $p_1 = 1/3$ as a reasonable and conservative threshold to identify potential Level-1 conflicts. An important observation is that the conflicts identified during the deterministic analysis correspond to aircraft trajectories actually having a very small probability of occurrence. Using a probabilistic analysis (with any satisfactory threshold probability) yields a significantly more robust prediction of potential aircraft conflicts, given that navigation errors do occur in practice.

Having selected a Level-1 threshold probability, we examined the total conflicts identified as a function of p_2, the threshold probability for identifying Level-2 conflicts. Table 7-11 presents the results obtained.

	Test Set 1		Test Set 2	
p_2	n_A = 15	n_A = 21	n_A = 15	n_A = 21
1/3	68	64	600	583
0.30	68	64	600	583
0.25	68	64	600	584
2/9	68	64	612	590
0.20	84	66	638	604
1/6	88	88	660	647
0.15	93	88	703	657

Table 7-11: Level 1 and 2 Conflicts Versus Threshold Probability

Based on these results, we selected $p_2 = p_1/2 = 1/6$ as a reasonable, conservative threshold for identifying Level-2 conflicts. Recall that the dimensions of the Level-2 separation box are ½ those of the Level-1 separation box, while the conflict probabilities are the product of two realization probabilities. Hence, we have taken the squares of the threshold probabilities to be in proportion to the respective cross-sectional box areas.

Observe in Tables 7-10 and 7-11 that throughout the range of threshold probabilities tested, a similar number of conflict intervals were identified using either n_A=15 or n_A=21 realizations in the horizontal plane. Upon inspection of the respective sets of conflict intervals, we found that the additional computational burden required when using n_A=21 realizations did not yield a substantially distinct conflict risk analysis

from that obtained using n_A=15 realizations. Therefore, we shall use the latter for model implementation.

Turning our attention to fatal conflict probabilities, observe that each trajectory displacement realization in the horizontal plane of Trajectory Displacement Sets 3 and 6, for example, are separated by a minimum geometric distance of more than 2000 feet (occurring in the cross-track dimension). The inviolable airspace around each focal aircraft (which, when pierced by an intruder aircraft defines a fatal conflict) extends 500 feet in the both the in-trail and cross-track axes. Given this fact, we expect that any fatal conflicts identified will have relatively small associated probabilities. This was the case with the two data sets examined for all of the rectangular trajectory displacement distributions. (Note that there are no identical or closely parallel flight plans included in either data set.) The average fatal conflict probabilities for each distribution ranged from 0.011 to 0.043. The maximum fatal conflict probability encountered was 0.0623.

The probabilistic displacement realizations for the wind-induced distributions are closer together geometrically, having a minimum separation distance of approximately 350 feet. Using these distributions with the two data sets yielded similar average fatal conflict probabilities as before. However, as expected, the maximum fatal conflict probability encountered was significantly higher, being 0.1518.

We therefore chose a conservative fatal threshold probability (consistent with our rationale for selecting p_1 and p_2) of $p_{\text{fatal}} = 1/18$. Note that this is greater than any of the averages of fatal conflict probabilities encountered in our experiments, but lesser than the maximum values of these fatal conflict probabilities.

To summarize, we have selected our baseline threshold probabilities to be

$$p_{\text{thresh}} = \{p_1, p_2, p_{\text{fatal}}\} = \left\{1/3, 1/6, 1/18\right\}. \tag{7.1}$$

Using these baseline threshold probabilities, Table 7-12 identifies the conflict information for the two test data sets.

	Test Set 1			Test Set 2		
Number of Flights	30			80		
Surrogates per Flight	6			6		
Trajectory Displacement Set	3	8	8	3	8	8
Realizations (Planar)	15	15	15	15	15	15
Wind Direction	n/a	SSW	N	n/a	SSW	N
Solution Time (seconds)	9.94	9.82	9.82	99.11	93.86	93.92
Probabilistic Conflicts						
Level 1:	28	8	20	242	117	275
Level 2:	60	42	27	415	446	393
Fatal:	4	0	0	7	4	7

Table 7-12: PAEM Computational Results

We shall later study the sensitivity of the APCDM solution to selecting more or less conservative thresholds (i.e., respectively, smaller or greater threshold probabilities).

7.2. Analysis of the C_3 and C_4 Conflict Constraint Formulations

In Section 4.7 we showed, via Proposition 4-5, that the C_4 formulation provides a tighter representation than the C_3 formulation. Using the two test data sets described in Section 7.1.1. plus the two additional test data sets described in Table 7-13, we verified the practical benefit of using the C_4 formulation, in terms of computational effort. For Test Sets 1 and 2, we generated several conflict constraint sets by varying the conflict threshold probabilities from their respective nominal values to relatively small values. In the latter case, this yielded relatively dense conflict sets. The resulting problem instances and their labels and specifications are presented in Table 7-14.

	Test Set 3		Test Set 4	
Number of Flights	100		120	
Surrogates per Flight	9		6	
Center(s)	ZMA/ZJX		ZMA/ZJX	
Number of Airlines	6		4	
Airlines: Flights per Airline	AAL: CAA: COA: DAL: DEL: UAL:	14 18 25 9 22 12	AAL: DAL: UAL: USA:	40 23 22 35
Time Horizon	200 min		1800 min	
Number of Deterministic Conflicts Identified	Level 1: Level 2: Fatal:	3999 5498 1285	Level 1: Level 2: Fatal:	1211 704 55

Table 7-13: Test Sets 3 and 4

Firstly, note that the C_4 formulation provides a more compact representation than the C_3 formulation, in terms of the number of constraints generated, as evident from Table 7-14.

Label	Test Set *	Edges in A	Maximum Number of Overlapping Sets of Conflicts in any Sector	Maximum Number of Conflicts in any Overlapping Set	Number of C_3 Constraints Generated	Number of C_4 Constraints Generated
CFT-1	1	44	3	9	59	25
CFT-2	1	283	18	20	453	207
CFT-3	2	477	23	17	725	262
CFT-4	2	573	24	18	933	314
CFT-5	2	1130	57	45	2621	667
CFT-6	2	1407	68	56	3601	830
CFT-7	2	1448	70	42	3537	895
CFT-8	3	1458	37	140	6351	653
CFT-9	4	1215	74	70	3675	711
CFT-10	4	1436	72	65	4230	870
* All instances use rectangular trajectory displacement regions, except for CFT-5 with a cylindrical, SSW wind-induced displacement region, and CFT-6 and CFT-10 with a cylindrical, N wind-induced displacement region.						

Table 7-14: C_3 Versus C_4 Constraints Generated

Second, to better examine the usefulness of the three conflict constraint formulations, we disabled the CPLEX program's automatic generation of various MIP cuts. Accordingly, using these options, we examined the overall computational effort required using the C_3 and C_4 formulations, and also compared this with the effort required by the C_2 formulation that has been implemented in the APM formulation of Sherali, Smith, and Trani [41]. The results of these experiments are displayed in Table 7-15.

Label *	$\overline{n}_s$	C_2 Solution Time (seconds)	C_3 Solution Time (seconds)	C_4 Solution Time (seconds)
CFT-1	15	0.781	0.821	0.771
CFT-2	15	1.041	1.321	1.191
CFT-3	15	9.303	9.623	7.661
CFT-4	15	11.276	9.834	9.053
CFT-5	15	28.711	44.423	30.253
CFT-6	15	45.835	83.516	61.338
CFT-7	15	26.978	55.147	29.752
CFT-8	15	65.844	**	73.666
CFT-9	15	314.952	**	274.504
CFT-10	15	357.574	**	295.240
CFT-1a	3	0.570	0.540	0.600
CFT-2a	3	0.831	0.931	0.971
CFT-3a	3	53.286	51.774	66.856
CFT-4a	3	59.475	71.793	60.206
CFT-5a	3	71.012	83.570	53.056
CFT-6a	3	188.581	294.418	160.661
CFT-7a	3	195.571	402.200	230.690
CFT-8a	7	723.670	**	772.506
CFT-9a #	9	632.138	**	276.407
CFT-10a #	9	301.493	**	207.888

* "a" label indicates an identical data set with sector capacity constrained as shown in next column
** Resulting constraint matrix size exceeded the computer's memory capacity
# Solution obtained using an LP/IP gap tolerance of 5%

Table 7-15: Computational Effort Using C_2, C_3, and C_4

The three formulations are indistinguishable, in terms of computational effort, for the first four instances and CFT-1a, while the C_3 formulation exhibits a more intense effort for the remaining instances, and is of an untenable size for CFT-8, CFT-9, and CFT-10. These first four problems were such that few of the conflict resolution

constraints produced any significant impact (given the allowable airspace traffic density) in that there were readily substitutable surrogates (albeit inferior in terms of cost) available to replace those that generated significant conflicts. For all of the instances, we obtained optimal solutions with zero flight cancellations, and with peak sector occupancy levels of n_s=5 for the first seven cases, n_s=8 for CFT-8, and n_s=12 for CFT-9 and CFT-10. In the case of CFT-5 through CFT-10, observe that the greatly increased size of the constraint matrix for the C_3 formulation places a significant computational burden on the overall model.

We limited the allowable simultaneous sector occupancies as shown by the $\overline{n}_s$ values in Table 7-15. This required a more careful selection of available surrogates, thereby increasing the impact of surrogates made unavailable due to the conflict resolution constraints. The net effect on the LP relaxation was to fractionate the variables representing the selection of key surrogate alternatives. Consequently, the potential effectiveness of the tighter C_4 formulation became more evident in the results for the instances CFT-9, CFT-10, CFT-5a, CFT-6a, CFT-9a, and CFT-10a, where C_4 resulted in an average savings of 29% of the effort required by C_2. These instances had a relatively high number of potential conflicts, and in the latter four cases, more restricted maximum occupancy constraints. On the other hand, for the instances CFT-3a, CFT-7a, and CFT-8a, C_2 resulted in a savings of 25%, 18% and 7%, respectively, of the effort required by C_4. In these instances, the trade-off between the tightness afforded by C_4 and its size gave C_2 an advantage because of the nature of the problems. Overall, we advocate using C_4 since its additional size does not significantly burden the model, while its relative tightness is advantageous when solving problems having more complex conflicting situations.

To illustrate the nature of the cuts from the C_3 and the C_4 formulations, let us examine in detail one of the conflict subgraphs that was generated for the instance CFT-3a, as shown in Figure 7-2.

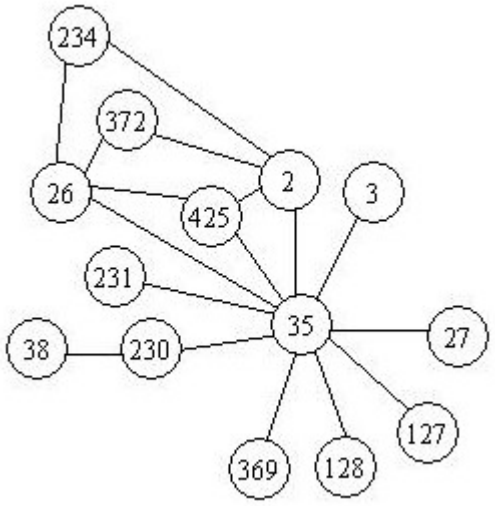

Figure 7-2: Conflict Subgraph Example

Suppose that we maximize the following weighted sum of node selections, where the weights correspond to the relative costs of the respective flight plans as follows:

$$\text{Maximize} \quad \left\{ \begin{matrix} x_2 + x_3 + 4.3\, x_{26} + x_{27} + 1.5\, x_{35} + 1.4\, x_{38} + 4.2\, x_{127} \\ + x_{128} + 1.7\, x_{231} + 4.5\, x_{234} + x_{369} + 2.7\, x_{372} + 2\, x_{425} \end{matrix} \right\}, \tag{7.2}$$

subject to the set of C_2 constraints corresponding to the Figure 7-2 conflict subgraph. The LP relaxation in this case yields the partial solution

$$\left\{ x_{26}, x_{234}, x_{372}, x_{425}, x_{35} \right\} = \left\{ 1/3, 1, 1, 1, 1 \right\}, \text{ and}$$

$$\left\{ z_{(26,234)}, z_{(26,372)}, z_{(26,425)}, z_{(26,35)} \right\} = \left\{ 1/3, 1/3, 1/3, 1/3 \right\}. \tag{7.3}$$

The remaining decision variables in this instance have integral values at optimality. Recalling (4.35) for the C_3 formulation, observe from Figure 7-2 that we can tighten the conflict constraint representation by adding, for example, either of the following T_{NC} cuts:

$$x_{26} + x_{234} + x_{425} \leq 2$$
$$x_{26} + x_{372} + x_{425} \leq 2\,. \tag{7.4}$$

Note that both these cuts delete the fractional LP solution. The resulting LP relaxation for the C_2 formulation, augmented with either of these two T_{NC} cuts, yields an optimal solution that is integral. Alternatively, referencing (4.62), we can add the following C_4 constraint, for example,

$$z_{(26,234)} + z_{(26,372)} + z_{(26,425)} + z_{(26,35)} \leq x_{26}\,. \tag{7.5}$$

Note that this cut also deletes the current fractional solution. When the LP relaxation for the foregoing C_2 formulation is augmented with (7.5), we again obtain an integral solution at optimality. However, to fully implement the C_3 formulation for this conflict subgraph, fifty-seven T_{NC} cuts are required, although a partial constraint generation scheme could be adopted. In contrast, only seven constraints are required to implement the C_4 formulation, which we showed via Proposition 4-5 to be yet a tighter representation than C_3. As demonstrated in Table 7-15, the large number of constraints required by the C_3 formulation can impose an unacceptable computational burden. Observe that even in cases where the conflict structure is such that the APCDM does not benefit from the C_4 cuts, the impact of these cuts to the overall computational effort is minimal. More importantly, the C_4 formulation offers a significant computational improvement for certain relatively dense conflict constraint structures, as observed above.

7.3. Analysis of the CDM Representation

7.3.1. Analysis of Varying the Parameter $D_{\max}$

Recall from Section 5.2 that the parameter $D_{\max}$ is the maximum allowable ratio for any airline of its cost pertaining to the set of surrogates selected through the CDM process to its individually optimized set of surrogates. We examined the sensitivity of the objective function value to progressively decreasing values of $D_{\max}$, using four instances of the APCDM, and beginning with $D_{\max}$=1.5 (an unreasonably high value,

since airlines would be unlikely to accept a 50% cost increase associated with participating in a group decision), and then moving to progressively lower values until $D_{\max}$=1.02. Figure 7-3 depicts the results obtained via this sensitivity analysis, using Test Sets 2 and 3.

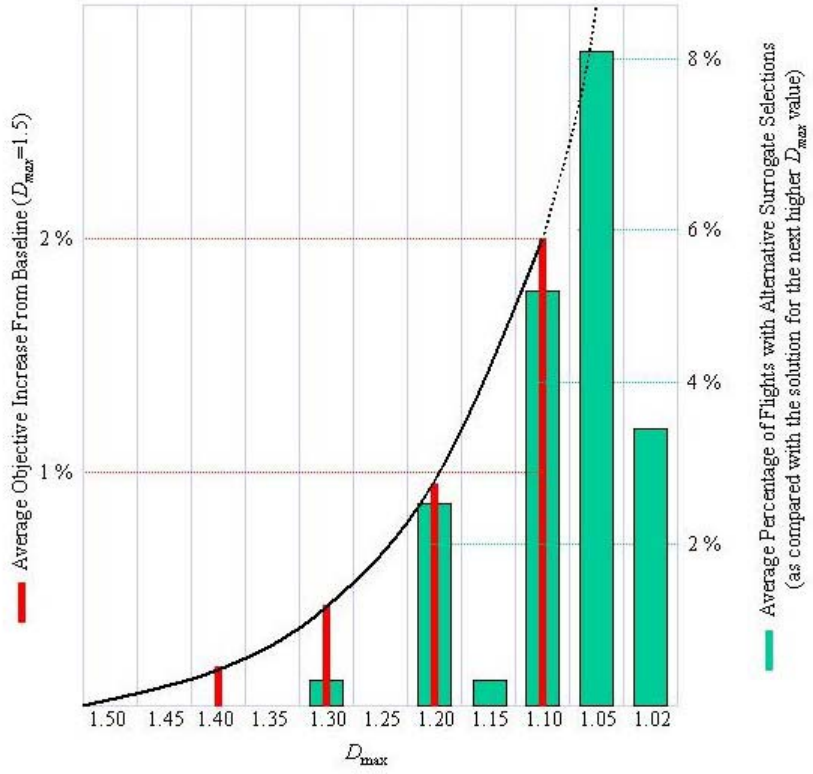

Figure 7-3: D_{max} Analysis

Observe that the objective function increases non-linearly as $D_{\max}$ decreases, but that the rate of this increase is quite small. Indeed, much of the increase can be directly attributed to the progressively steeper slope of the airline efficiency curve (5.10) that occurs as $D_{\max}$ is decreased. Observe that, as the slope of this curve is made steeper, any change in surrogate selection will yield a relatively greater impact on airline collaboration efficiency. Hence, as expected, we noted a corresponding increase in the solution's ω-mean collaboration equity as $D_{\max}$ was decreased. To gain further insights, we examined the impact $D_{\max}$ had on the selection of surrogates for the various flights. Specifically, we determined the number of flights where a different surrogate was

selected at optimality from the one selected when $D_{\max}$ was at the next higher level. Referring to Figure 7-3, observe that for $D_{\max}$>1.2, this parameter has little impact on the surrogates selected. Below this value, the optimal selection of surrogates becomes sensitive to the value of $D_{\max}$. By examining the APCDM output more closely, we noted a generalized trend towards an increase in the average and peak sector occupancies and in the number of resolvable conflicts as $D_{\max}$ decreased. This translated to an increase in the sector monitoring and conflict resolution (penalty) costs, and an increase in the efficiency-based penalty costs for decreasing values of $D_{\max}$. (For example, when $d_\alpha(x)$=1.05, say, we have a corresponding airline efficiency for airline α equal to 95% when $D_{\max}$ =1.5, whereas this efficiency is 50% when $D_{\max}$=1.10. The latter case yields an objective penalty that is 10 times that of the former case.)

For APCDM implementation, we chose $D_{\max}$=1.20. This is a reasonable upper limit for collaboration costs that would likely be acceptable by participating airlines. This value also reflects a level where this parameter can be expected to influence the selection of surrogates at optimality.

7.3.2. Analysis of Varying the Parameter $E^e_{\max}$

Having selected $D_{\max}$=1.20, we examined next the unconstrained airline collaboration equities and the ω-mean collaboration equity, plus the ω-mean collaboration efficiency, that were achieved at optimality for each of four APCDM instances. The results are displayed in Table 7-16.

APCDM Instance	$\sum_\alpha \omega_\alpha E_\alpha(x)$	$\max_\alpha \{E^e_\alpha(x)\}$	x^e
CDM-1	0.9608	0.0187	0.0070
CDM-2	0.9474	0.0321	0.0087
CDM-3	0.5014	0.1867	0.0612
CDM-4	0.9928	0.0437	0.0024

Table 7-16: CDM Values at Optimality (Unconstrained Equity)

The three instances with optimal solutions having a higher ω-mean collaboration efficiency also yielded a relatively small ω-mean collaboration equity. Next, we focused

the analysis on instance CDM-3, and the sensitivity of its solution to reductions in the upper bound for airline collaboration equities, $E^e_{\max}$. Table 7-17 shows the values obtained for the ω-mean collaboration efficiency, the ω-mean collaboration equity, and the changes in the objective (relative to that obtained via an unconstrained $E^e_{\max}$) as $E^e_{\max}$ is decreased.

$E^e_{\max}$	Unconstrained	0.15	0.10	0.08	0.06	0.04	0.02
$\sum_\alpha \omega_\alpha E_\alpha(x)$	0.5013	0.4989	0.4953	0.4955	0.4822	0.4818	0.4760
x^e	0.0612	0.0574	0.0523	0.0442	0.0337	0.0217	0.0042
% Objective Increase with Respect to Objective with Unconstrained $E^e_{\max}$	0%	0.04%	0.09%	0.18%	0.32%	0.35%	0.41%

Table 7-17: $E^e_{\max}$ Sensitivity Analysis

Observe from the general tendency as $E^e_{\max}$ decreases that the gains (reductions in "spread") in ω-mean collaboration equity more than offset the ω-mean collaboration efficiency losses. To comply with the more stringent equity requirement (created by having imposed a lower upper bound on airline collaboration equities), there is a corresponding loss of flexibility in the surrogates that may be chosen for the solution. Hence, in general, more costly surrogates were chosen. However, the impact on the overall solution cost was greatly mitigated by the reduced penalties accruing from the tradeoff between the ω-mean collaboration efficiency and the ω-mean collaboration equity.

We chose $E^e_{\max}$ =0.08 for APCDM implementation. This bound impacts the objective function to a lesser extent than does $D_{\max}$. Note that for three of the APCDM instances, the unconstrained airline collaboration equities are below this threshold, hence no additional cost was incurred. Figure 7-4 shows the relationship between $E^e_{\max}$

and the potential collaboration cost to be borne by each respective airline. For example, if some instance of the APCDM yields an optimal ω-mean collaboration efficiency of $\sum_{\alpha} \omega_{\alpha} E_{\alpha}(x)$=0.5, say, then with $\left|E^{e}_{\alpha}(x)\right| \le E^{e}_{\max} = 0.08$, and $D_{\max}$ =1.2, we can determine that airline α will have incurred a collaboration cost between 8.4% and 11.6% of its respective individually optimized costs.

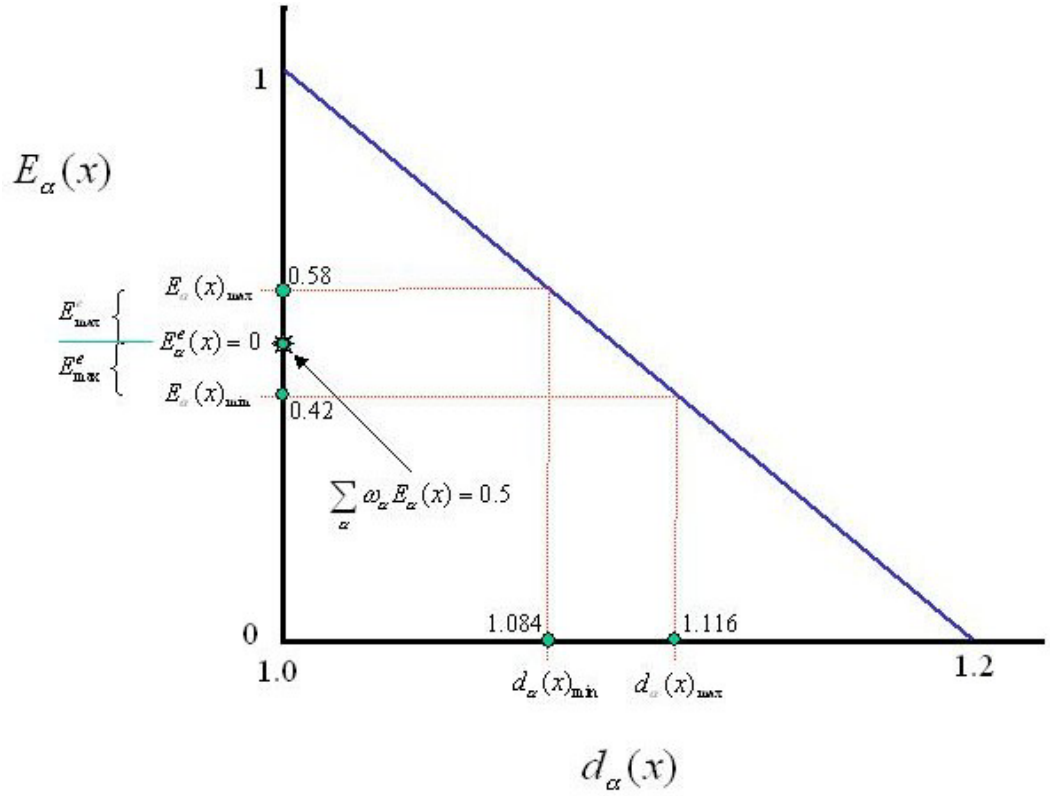

Figure 7-4: Relationship Between $E^{e}_{\max}$ and $d_{\alpha}(x)$

7.3.3. Analysis of Varying the Parameter μ_0

Recall from (6.6) in Section 6.2.4. that we selected the constant μ_0=0.1 to use within the penalty functions corresponding to the levels of the ω-mean collaboration efficiency and the ω-mean collaboration equity achieved. Here, we assess the effect of this parameter μ_0 on the APCDM solution. Specifically, using the APCDM instances cited in Table 7-16, we examined the effect of the parameter μ_0 on the ω-mean collaboration efficiency and the ω-mean collaboration equity for the resulting solutions.

Since we weighted the two CDM measures equally (i.e., we used $\mu^e = \mu^D$ in (6.6)), we averaged the improvements exhibited for these measures as μ_0 was increased from zero to 0.3. For any value of $\mu_0 = \bar{\mu}_o$ define the *Average CDM Improvement* as

$$0.5\left[\left\{\sum_{\alpha=1}^{\bar{\alpha}}\omega_\alpha E_\alpha(x)\right\}_{\mu_0=\bar{\mu}_0} - \left\{\sum_{\alpha=1}^{\bar{\alpha}}\omega_\alpha E_\alpha(x)\right\}_{\mu_0=0}\right] + 0.5\left[\left\{x^e\right\}_{\mu_0=0} - \left\{x^e\right\}_{\mu_0=\bar{\mu}_0}\right]. \qquad (7.6)$$

Figure 7-5 depicts the results of this analysis, where the *Average Percentage CDM Improvement* is given by (7.6) expressed as a percentage of

$$0.5\left\{\sum_{\alpha=1}^{\bar{\alpha}}\omega_\alpha E_\alpha(x)\right\}_{\mu_0=0} + 0.5\left\{x^e\right\}_{\mu_0=0}.$$

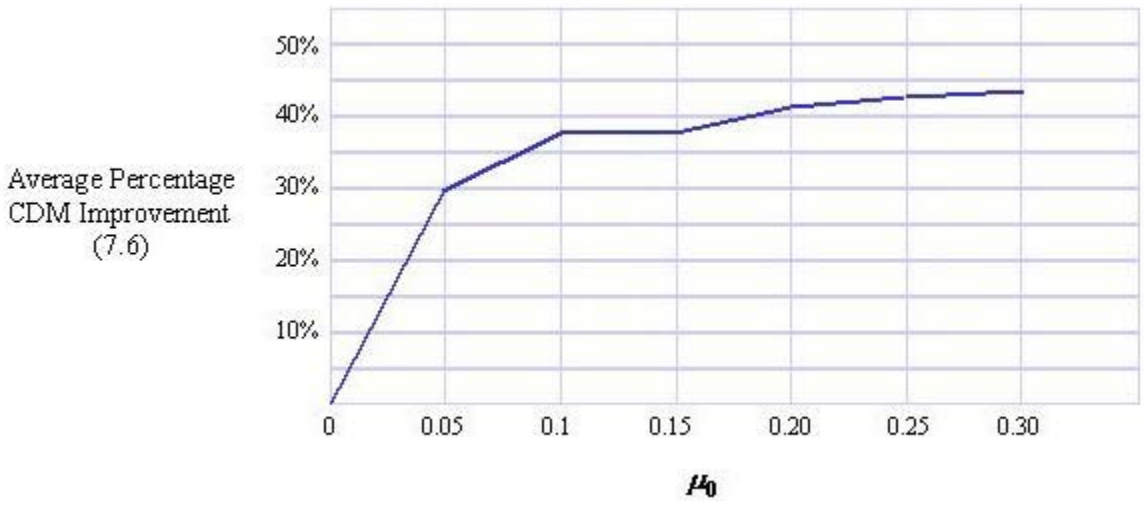

Figure 7-5: Sensitivity Analysis with Respect to μ_0

The intent of the CDM penalty terms in the objective function is to create a mathematical incentive to choose solutions that include an adequate consideration of CDM issues, namely, ω-mean collaboration efficiency and ω-mean collaboration equity. Figure 7-5 makes evident that this goal is substantially achieved at μ_0=0.1. By increasing μ_0 further, we obtain only marginal gains in the ω-mean collaboration

efficiency and the ω-mean collaboration equity, while significantly increasing the objective (as much as 9% from the objective where μ_0=0), thereby substantially masking the direct costs that are incurred by the airlines. We conclude, therefore, that our initial selection of μ_0=0.1 was appropriate.

7.4. Analysis of Varying the Conflict Risk Threshold Probabilities

We performed this analysis using Test Sets 2 and 3. Recall that these sets consist of 80 flights with six surrogates each, and 100 flights with nine surrogates each, respectively. The sector capacity was nominally restricted with $\overline{n}_s$ =15, $\forall s$=1,…,S for Test Set 2 and moderately constrained with $\overline{n}_s$ =9, $\forall s$=1,…,S for Test Set 3. Five experiments, using the threshold probabilities shown in Table 7-18, were performed for each set. Note that the thresholds for level-one, level-two, and fatal conflicts, respectively, were varied proportionally. The results of this experiment are displayed in Table 7-19.

	p_1	p_2	p_{fatal}
TP-1	0.3733	0.1867	0.05956
TP-2	0.3533	0.1767	0.05756
TP-3	0.3333	0.1667	0.05556
TP-4	0.3133	0.1567	0.05356
TP-5	0.2933	0.1467	0.05156

Table 7-18: Conflict Risk Threshold Probabilities

Test Set	Threshold Probability Set	|A|	Total Objective Value	$\sum_{\alpha} \omega_{\alpha} E_{\alpha}(x)$	x^e	Conflicts
2	TP-1	371	$ 126,960	0.9203	0.0400	6
	TP-2	418	$ 127,199	0.9086	0.0355	6
	TP-3	477	$ 127,262	0.9086	0.0355	6
	TP-4	520	$ 127,284	0.8653	0.0310	6
	TP-5	582	$ 127,296	0.8653	0.0310	6
3	TP-1	1286	$ 153,276	0.6020	0.0375	7
	TP-2	1372	$ 153,429	0.6009	0.0309	5
	TP-3	1458	$ 153,461	0.5913	0.0213	5
	TP-4	1543	$ 154,357	0.5827	0.0213	6
	TP-5	1666	$ 153,476	0.6008	0.0340	5

Table 7-19: Threshold Probability Sensitivity Analysis

We found that the objective value, the ω-mean collaboration efficiency, and the ω-mean collaboration equity were all insensitive to changes in the conflict risk threshold probabilities for both data sets. For example, the TP-2 and TP-3 instances for Test Set 2 yielded identical decisions. However, observe that the objective value for the TP-3 case is $63 greater than that for TP-2. The reason for this is that the relatively lower conflict risk threshold probabilities in TP-3 resulted in one of the conflicts being "upgraded" from a level-one to a level-two conflict. Recall Equation (6.5), which assigns the penalty cost associated with resolvable conflicts included in the solution. Even for a severity level-two conflict, the penalty cost of $84.24 is, in general, relatively small with respect to the direct costs that would be associated with selecting alternative surrogates that might be necessary to avoid the conflicts. Furthermore, selecting alternative surrogates might also impose significant penalties corresponding to a decrease in the ω-mean collaboration efficiency or an increase in the ω-mean collaboration equity. Hence, allowing additional resolvable conflicts within capacity limits will be typically preferred to selecting alternative surrogates.

To gain further insights, we repeated the two experiments by prohibiting all conflicts, even resolvable ones, from the solution (i.e., setting r_s=0, $\forall s$=1,…,S, in (6.2a,b)). The results of this experiment are shown in Table 7-20.

Test Set	Threshold Probability Set*	Total Objective Value	$\sum_{\alpha} \omega_{\alpha} E_{\alpha}(x)$	x^e
2	TP-1a	$ 129,019	0.8409	0.0296
	TP-2a	$ 129,193	0.7996	0.0215
	TP-3a	$ 129,908	0.7753	0.0157
	TP-4a	$ 131,217	0.7378	0.0307
	TP-5a	$ 131,426	0.7274	0.0510
3	TP-1a	$ 156,449	0.5169	0.0088
	TP-2a	$ 156,262	0.5274	0.0181
	TP-3a	$ 156,771	0.5092	0.0013
	TP-4a	$ 156,620	0.5182	0.0077
	TP-5a	$ 156,531	0.5189	0.0100
* "a" label indicates identical data sets from Table 7-19 with all conflicts prohibited from the solution				

Table 7-20: Threshold Probability Sensitivity Analysis (with r_s=0, $\forall s$=1,…,S)

Both the ω-mean collaboration efficiency and the ω-mean collaboration equity trended towards slightly inferior values for Test Set 2, but there was not any identifiable trend for Test Set 3. The APDCM objective trended upward as the threshold probabilities were decreased for Test Set 2, but only marginally. That is, varying the conflict threshold probabilities by $\pm$12% from their nominal values of $\{p_1, p_2, p_{fatal}\}$ = {1/3, 1/6, 1/18}, as shown in Table 7-18, yielded only an objective function change of [-0.68%, 1.17%] for Test Set 2. Note that for Test Set 3 there was no sustained objective function increase across the range of threshold probabilities, despite the relatively more constrained conditions versus those in Test Set 2. These results indicate that the mix of available surrogates for these test instances is rich enough to provide a comparable tradeoff between the two CDM penalty functions and the direct costs of the selected surrogates. Although additional data sets might be useful to further establish these findings, our preliminary conclusion is that the overall APCDM is not particularly sensitive to moderate changes in the conflict risk threshold probabilities.

The foregoing conclusion does not diminish the significance of the contribution of our stochastic conflict risk analysis (versus the prior deterministic approach) to the overall APCDM. Recall from the discussion in Section 7.1.3. that the conflicts identified

during the deterministic analysis correspond to aircraft trajectories actually having a very small probability of occurrence and that the probabilistic analysis yields a significantly more robust prediction of potential aircraft conflicts. Our experiments show that this robustness is not adversely affected, within reasonable limits, by the particular selection of threshold probabilities.

7.5. Summary of Computational Results

Table 7-21 summarizes the final parameterization for the APCDM.

Parameter	Value	Description
p_1	0.3333	Conflict risk threshold probability for level-one conflicts
p_2	0.1667	Conflict risk threshold probability for level-two conflicts
p_{fatal}	0.0556	Conflict risk threshold probability for fatal conflicts
$D_{\max}$	1.2	Maximum allowable ratio for airline cost pertaining to the set of surrogates selected through CDM process to its individually optimized set of surrogates
$E^e_{\max}$	0.08	Maximal ω-mean collaboration equity
μ_0	0.1	CDM penalty function constant

Table 7-21 : APCDM Parameterization

Using the foregoing parameters, we performed runs (one using randomized trajectory displacements in the rectangular bounded region, and two using the wind-induced displacements in the cylindrical bounded region) for each of the first two test data sets. As a point of comparison, we also ran the case of deterministic trajectories to assess its relative impact on costs, workload, efficiencies, and equity measures. For the Test Set 3, we include a run for a case of rectangular displacement regions. Because of the artificially high number of conflicts created by this data set, the PAEM identified 10782, 4353, and 5271 conflict intervals for the Test Set 3 Deterministic, Northerly wind-induced Cylindrical, and South-southwesterly wind-induced Cylindrical instances, respectively, and the resulting problem sizes exceeded the available

computer memory resources. We shall leave these for future investigation using a more advanced platform. Table 7-22 summarizes the computational results obtained.

Test Set	Probabilistic Trajectory Displacement Region	$\|A\|$	Total Objective Value	$\sum_{\alpha} \omega_{\alpha} E_{\alpha}(x)$	x^{e}	Total Resolvable Conflicts in Solution	CPLEX Computational Time (seconds)
1	Deterministic	58	$ 53,425	0.9744	0.0341	0	1.141
1	Rectangular	44	$ 53,475	0.9485	0.0531	0	1.822
1	Cylindrical N-wind	34	$ 53,425	0.9744	0.0341	0	1.071
1	Cylindrical SSW-wind	29	$ 53,425	0.9744	0.0341	0	1.111
2	Deterministic	597	$ 127,098	0.9120	0.0485	10	23.173
2	Rectangular	477	$ 127,262	0.9086	0.0355	6	25.036
2	Cylindrical N-wind	406	$ 126,331	0.9306	0.0475	3	15.942
2	Cylindrical SSW-wind	475	$ 126,387	0.9342	0.0497	6	14.741
3	Rectangular	1458	$ 138,711	0.9897	0.0048	3	67.296
4	Deterministic	1306	$ 140,071	0.3313	0.0431	23	319.339
4	Rectangular	1436	$ 140,409	0.3580	0.0234	27	252.372
4	Cylindrical N-wind	1215	$ 140,805	0.1528	0.0144	20	276.207
4	Cylindrical SSW-wind	1345	$ 140,905	0.2549	0.0093	27	290.277

Table 7-22: Computational Summary

Observe that each of the instances yielded a solution having a low ω-mean collaboration equity. However, the Test Set 4 instances were such that, relative to the other test sets, the solutions yielded a low ω-mean collaboration efficiency along with a significant number of conflicts. This can be attributed to the specific nature of the flight plans in the data set. Also, there were no cancelled flights, and sector capacities were

not a limiting factor for any of these nine instances. The peak occupancy observed was n_s=14 in one sector, occurring in the Test Set 3 instance.